Article

Molecular Cell

ULK1/2 Constitute a Bifurcate Node Controlling Glucose Metabolic Fluxes in Addition to Autophagy

Graphical Abstract

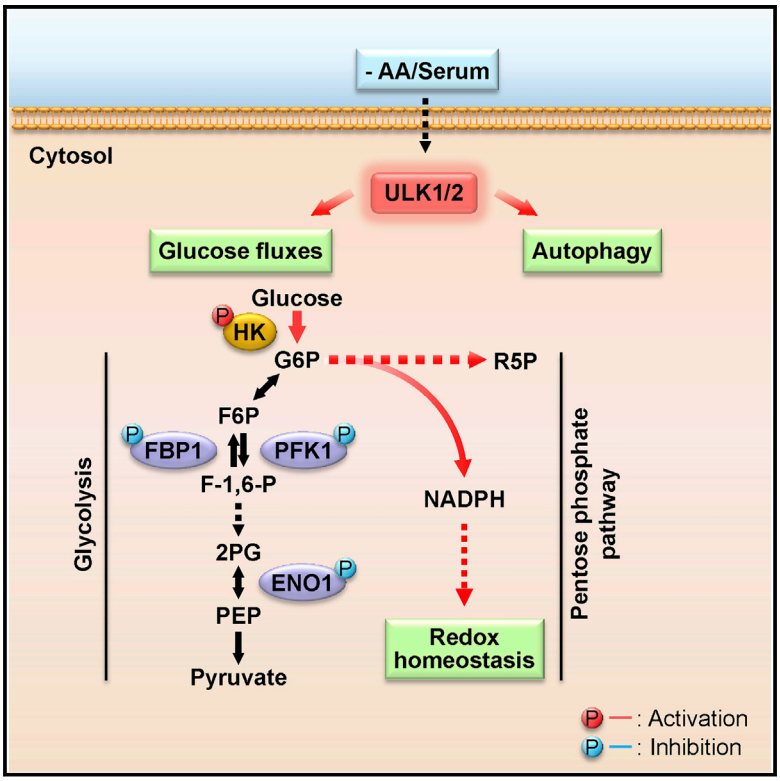

Highlights

- ULK1/2 deficiency leads to reduction of glycolysis during nutritional stresses
- HK1, PFK1, FBP1, and ENO1 are direct substrates of the ULK1 kinase
- ULK1 regulates activities of glycolytic enzymes and sustains glycolysis and PPP flux
- ULK1/2 reprogram glucose metabolic fluxes independently of autophagy

Authors

Terytty Yang Li, Yu Sun, Yu Liang, ..., Shu-Yong Lin, Daniel Tsun-yee Chiu, Sheng-Cai Lin

Correspondence

linsc@xmu.edu.cn

In Brief

Metabolic reprogramming underlies adaptive responses to various stresses. Li et al. discover that the autophagy-initiating kinases ULK1/2 also phosphorylate multiple glycolytic enzymes to sustain glycolysis and increase the proportion of glucose flux to the pentose phosphate pathway during nutritional stresses.

Li et al., 2016, Molecular Cell 62, 359–370
May 5, 2016
http://dx.doi.org/10.1016/j.molcel.2016.04.009

Molecular Cell
Article

ULK1/2 Constitute a Bifurcate Node Controlling Glucose Metabolic Fluxes in Addition to Autophagy

Terytty Yang Li,[1] Yu Sun,[1] Yu Liang,[1] Qing Liu,[1] Yuzhe Shi,[1] Chen-Song Zhang,[1] Cixiong Zhang,[1] Lintao Song,[1] Pu Zhang,[2] Xianzhong Zhang,[2] Xiaotong Li,[1] Tao Chen,[1] Hui-Ying Huang,[1] Xiadi He,[3] Yi Wang,[4] Yu-Qing Wu,[1] Shaoxuan Chen,[1] Ming Jiang,[1] Canhe Chen,[1] Changchuan Xie,[1] James Y. Yang,[1] Yan Lin,[3] Shimin Zhao,[3] Zhiyun Ye,[1] Shu-Yong Lin,[1] Daniel Tsun-yee Chiu,[5,6] and Sheng-Cai Lin[1,*]

[1]State Key Laboratory of Cellular Stress Biology, Innovation Center for Cell Signaling Network, School of Life Sciences, Xiamen University, Fujian 361102, China

[2]Center for Molecular Imaging and Translational Medicine, State Key Laboratory of Molecular Vaccinology and Molecular Diagnostics, School of Public Health, Xiamen University, Fujian 361102, China

[3]State Key Laboratory of Genetic Engineering, School of Life Sciences, Fudan University, Shanghai 200032, China

[4]Institutes of Biomedical Science, Fudan University, Shanghai 200032, China

[5]Department of Medical Biotechnology and Laboratory Science, College of Medicine, Chang Gung University, Kwei-san, Tao-yuan 333, Taiwan

[6]Department of Laboratory Medicine, Chang Gung Memorial Hospital, Tau-yuan 333, Taiwan

*Correspondence: linsc@xmu.edu.cn

http://dx.doi.org/10.1016/j.molcel.2016.04.009

SUMMARY

Metabolic reprogramming is fundamental to biological homeostasis, enabling cells to adjust metabolic routes after sensing altered availability of fuels and growth factors. ULK1 and ULK2 represent key integrators that relay metabolic stress signals to the autophagy machinery. Here, we demonstrate that, during deprivation of amino acid and growth factors, ULK1/2 directly phosphorylate key glycolytic enzymes including hexokinase (HK), phosphofructokinase 1 (PFK1), enolase 1 (ENO1), and the gluconeogenic enzyme fructose-1,6-bisphosphatase (FBP1). Phosphorylation of these enzymes leads to enhanced HK activity to sustain glucose uptake but reduced activity of FBP1 to block the gluconeogenic route and reduced activity of PFK1 and ENO1 to moderate drop of glucose-6-phosphate and to repartition more carbon flux to pentose phosphate pathway (PPP), maintaining cellular energy and redox homeostasis at cellular and organismal levels. These results identify ULK1/2 as a bifurcate-signaling node that sustains glucose metabolic fluxes besides initiation of autophagy in response to nutritional deprivation.

INTRODUCTION

Metazoan cells rely on balanced availability of nutrients including glucose and amino acids as well as growth factors to maintain cell growth and survival. By degrading internal cellular components, autophagy functions to replenish anabolic substrates and energy under nutrient-poor or other stress conditions as well as in diverse pathophysiological processes (Choi et al., 2013; Rabinowitz and White, 2010; Wang et al., 2010; Xie and Klionsky, 2007). Genetic delineation of the critical components for autophagy has revealed numerous factors (Galluzzi et al., 2014; Mizushima et al., 2011; Nakatogawa et al., 2009), among which unc-51-like kinase 1 and 2 (ULK1/2) play an initiating role by coupling signals from nutrient-sensing proteins, including mechanistic target of rapamycin (mTOR) and AMP-activated protein kinase (AMPK) to the downstream autophagic factors, leading to the formation of autophagosomes (Egan et al., 2011; Kim et al., 2011; Jung et al., 2009). However, whether ULK1/2 may act as a multi-branching node connecting nutritional stress signals to other metabolic pathways, such as the pathways for glucose metabolism, remains unknown.

Glucose is the most-common source of energy for almost all living organisms, and exquisite mechanisms in the regulation of glucose metabolic fluxes have been evolved to enable cells to meet different intrinsic growth requirements or to adapt to variations of extracellular nutritional supply (Hammerman et al., 2004; Levine and Puzio-Kuter, 2010; Wellen and Thompson, 2012). In mammalian cells, glucose catabolism starts with its conversion to glucose-6-phosphate (G6P), which is catalyzed by hexokinase (HK), a rate-limiting step of glycolysis (Wilson, 2003). G6P is the branch point for proceeding to glycolysis or the pentose phosphate pathway (PPP) or to be stored as glycogen in certain type of cells. For glycolysis, G6P is first isomerized to fructose-6-phosphate (F6P) that is further converted into fructose-1,6-bisphosphate (F-1,6-P) by phosphofructokinase 1 (PFK1), the committed step of glycolysis (Mor et al., 2011). Following the split of F-1,6-P into two trioses by aldolases, enolase 1 (ENO1) functions in the conversion of 2-phosphoglycerate (2PG) to phosphoenolpyruvate (PEP), the ninth and penultimate step of glycolysis (Díaz-Ramos et al., 2012). FBP1 reverses the reaction catalyzed by PFK1 and plays a vital role in gluconeogenesis. Recent studies also revealed that inhibition of FBP1 enzymatic activity strongly increases glycolysis both in non-transformed and tumor cells (Dong et al., 2013; Li et al., 2014).

The PPP shunt is considered as the major contributor of reducing equivalents in the form of reduced nicotinamide adenine dinucleotide phosphate (NADPH) for reductive biosynthesis and maintaining cellular redox homeostasis (Fan et al., 2014). Inborn errors in PPP have been observed to be associated with various diseases such as fava-bean-induced hemolytic anemia, known as favism, which is caused by the deficiency of G6P dehydrogenase (G6PD), an X-linked recessive genetic condition that is particularly common in people of Mediterranean and African origin (Beutler, 2008). G6PD is the rate-limiting enzyme that catalyzes the initial step of the PPP shunt, oxidizing G6P to phosphogluconolactone while nicotinamide adenine dinucleotide phosphate ($NADP^+$) is reduced to NADPH. Regulation of glycolytic enzymes to increase the PPP flux has been demonstrated as an important way for cells to adapt to various stresses (Bensaad et al., 2006; Yi et al., 2012; Anastasiou et al., 2011).

Here, by combining in vitro reconstitution assays, generation of phospho-specific antibodies, and genetic manipulation, we identify HK, PFK1, FBP1, and ENO1 in the glucose metabolic pathways as direct phosphorylation substrates of ULK1/2. Phosphorylation of these enzymes occurs virtually only under nutritional stresses. Metabolomic analyses illustrate that, besides their classical role in the induction of autophagy to recycle cellular components to sustain energy supply and limit the generation of reactive oxygen species (ROS) during nutritional stresses, ULK1/2 function in the maintenance of intracellular energy and redox balance by allocating more G6P to the PPP to promote the generation of reducing potential for ROS detoxification while sustaining overall glucose catabolism. These findings establish an important adaptive mechanism for the reprogramming of glucose metabolic fluxes in response to nutrient deprivation, and understanding of this regulatory mechanism may offer us new strategies for prevention and treatment of human metabolic diseases.

RESULTS

Depletion of ULK1/2 Leads to Reduction of Glycolytic Flux during Amino Acid and Serum Starvation

To explore a possible link between ULK1/2 activation and regulation of glucose metabolism, we first knocked down *ULK1* and *ULK2* separately or together in the human colorectal cancer HCT116 cells (Figure 1A). Despite the presence of glucose, ULK1/2 can be activated upon deprivation of amino acid and/or serum (Lin et al., 2012; Russell et al., 2013; Shang et al., 2011). We found that, whereas knockdown of either *ULK1* or *ULK2* singly led to a moderate reduction in the rates of glucose consumption and lactate production in starvation medium lacking both amino acid and serum, *ULK1* and *ULK2* double knockdown (*ULK1/2* DKD) resulted in a severe reduction of glycolytic flux (Figure 1A), indicating that both ULK1 and ULK2 are involved in the maintenance of glucose catabolism. Similarly, depletion of ULK1/2 in human osteosarcoma U2OS cells, human breast cancer MCF7 cells, or mouse embryonic fibroblasts (MEFs) also resulted in significant reduction of glucose utilization during the starvation (Figures 1B and S1A–S1E), demonstrating that ULK1/2 play a general role in regulating glucose metabolism in various cell types. Likewise, wild-type (WT) cells also displayed higher glucose consumption and lactate production than cells depleted of ULK1/2 after treatment of rapamycin that activates ULK1 by inhibiting mTORC1-mediated phosphorylation at Ser^{758} (Figure S1F). Moreover, reconstitution of the *ULK1/2* DKD cells with WT-ULK1, but not with its catalytically inactive (KI) form, restored the glycolytic flux during starvation (Figures 1C and S1G).

The kinase activities of ULK1/2 are highly dependent on their assembling into an ~3-MDa complex with at least FIP200, ATG13, and ATG101 subunits, and depletion of any of these components would render ULK1/2 inactive (Hara et al., 2008; Hosokawa et al., 2009a, 2009b). We therefore knocked down these genes in HCT116 cells separately (Figures S1H–S1J) and observed similar reduction of glycolytic flux to that caused by depletion of ULK1/2 (Figures 1D and S1L). To assess whether the attenuation of glucose catabolism was directly caused by the decrease of autophagic activity resulting from the disruption of ULK1/2 complex, several downstream genes essential for autophagy (Galluzzi et al., 2014; Mizushima et al., 2011; Rabinowitz and White, 2010; Xie and Klionsky, 2007), including *ATG5*, *ATG7*, and *BECN1*, were separately knocked down (Figure S1K). Interestingly, no significant changes of glucose consumption and lactate production were detected in the knockdown cells compared to the control cells (Figures 1D and S1L). Similar results were also obtained using $Atg5^{-/-}$ MEFs (Figures 1E and S1M), in which conventional autophagy is fully blocked (Kuma et al., 2004). Together, these results indicate an important role of ULK1/2 in the regulation of glycolytic flux independent of the downstream autophagic events.

We next assayed the activities of enzymes in the glycolytic pathway by using lysates from control and *ULK1/2* DKD HCT116 cells placed either in complete medium or medium deprived of both amino acid and serum. Intriguingly, it was found that starvation led to increased catalytic activity of HK but reduced activity of PFK1. Reduced activities caused by starvation were also detected for FBP1 and ENO1. Meanwhile, the changes of the activities of the four enzymes after starvation did not occur in *ULK1/2* DKD cells (Figures 1F–1I). We also performed similar experiments in WT and $Ulk1/2^{-/-}$ MEFs and found again that, in the absence of *Ulk1/2*, these metabolic enzymes were much less sensitive to starvation (except that the activity of FBP1 in MEFs was too low to be detected; Figures S1N–S1Q). Of note, the activities of many other metabolic enzymes, such as phosphoglycerate kinase (PGK) or G6PD, did not show significant variation in either control or *ULK1/2* DKD cells (Figures S1S and S1T). Importantly, total protein levels for all the metabolic enzymes tested were unchanged (Figures 1J, S1R, and S1U). In addition, the enzymatic activities of HK, PFK1, and ENO1 changed similarly during starvation in $Atg5^{-/-}$ MEFs to those in the WT MEFs (Figures S1V–S1Z), confirming that autophagic activity per se is not required for the regulation of glycolytic flux during amino acid and serum starvation.

ULK1 Directly Phosphorylates Glycolytic Enzymes and Affects Their Enzymatic Activities

We next asked whether HK, PFK1, FBP1, and ENO1 could be the direct substrates for the serine/threonine kinases ULK1/2. Co-expression of WT, but not the KI form of, ULK1 with representative

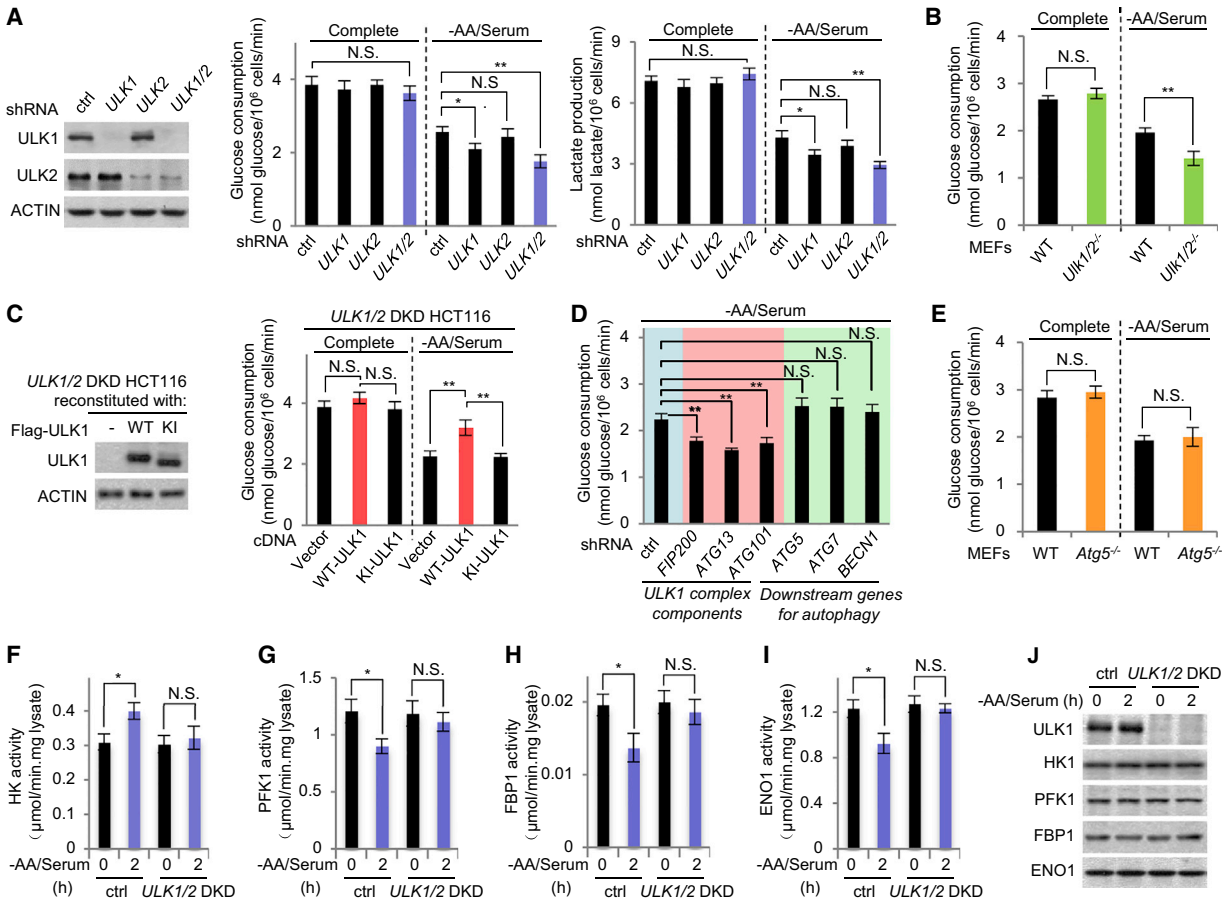

Figure 1. ULK1/2 Deficiency Leads to Reduction of Glycolytic Flux during Amino Acid and Serum Starvation

(A) Lentivirus-mediated knockdown of *ULK1* and/or *ULK2* (left). ACTIN was used as a loading control. Glucose consumption (center) and lactate production (right) of HCT116 cells expressing control shRNA (ctrl) or shRNAs targeting *ULK1* and/or *ULK2* in complete medium or medium free of amino acid and serum (n = 4 experiments) are shown.

(B) Glucose consumption of WT or *Ulk1/2*$^{-/-}$ MEFs placed in complete medium or medium free of amino acid and serum (n = 4 experiments).

(C) Reconstitution of WT-ULK1 or KI-ULK1 in *ULK1/2* double knockdown (*ULK1/2* DKD) cells (left). Glucose consumption (right) of *ULK1/2* DKD cells reconstituted with WT-ULK1, KI-ULK1, or empty vector in complete medium or medium free of amino acid and serum (n = 4 experiments) is shown.

(D) Glucose consumption of HCT116 cells with shRNA targeting *FIP200*, *ATG13*, *ATG101*, *ATG5*, *ATG7*, or *BECN1* in medium free of amino acid and serum (n = 4 experiments).

(E) Glucose consumption of WT or *Atg5*$^{-/-}$ MEFs placed in complete medium or medium free of amino acid and serum (n = 4 experiments).

(F–I) Enzyme activities of HK (F), PFK1 (G), FBP1 (H), and ENO1 (I) in control (ctrl) or *ULK1/2* DKD HCT116 cells placed in complete medium or medium free of amino acid and serum for 2 hr (n = 5 assays).

(J) Immunoblotting for the protein levels of the enzymes described in (F)–(I).

Error bars denote SEM. Statistical analysis was performed by ANOVA followed by Tukey in (A), (C), (D), and (F)–(I) and by Student's t test in (B) and (E) (*p < 0.05; **p < 0.01; N.S., not significant). See also Figure S1.

forms of these four metabolic enzymes resulted in different electrophoretic mobility shifts in gels containing Phos-tag that retards the mobility of phosphorylated proteins (Figure 2A; Kinoshita et al., 2006). Treatment of the immunoprecipitated enzymes with calf-intestinal alkaline phosphatase (CIP) effectively diminished the upper bands (Figure 2A). In vitro kinase assays using purified bacterially expressed metabolic enzymes and purified His-tagged ULK1 expressed in insect cells further confirmed that ULK1 could directly phosphorylate these enzymes (Figure 2B). Similar results were also obtained using ULK2 as the kinase (data not shown).

The four phosphorylated enzymes were then subjected to mass spectrometry, and multiple phosphorylated serine residues for each enzyme were identified (Figures S2A–S2D). Mutants carrying alterations of these serine residues to alanine singly or in combination were then constructed. It was found that, for HK1, combined mutation of Ser^{124} and Ser^{364} to alanine strongly diminished the phosphorylation signal (Figure 2C); for PFK1 (M isoform), Ser^{74} and Ser^{762} were identified to be the critical residues (Figure 2D); for FBP1, simultaneous mutation of Ser^{63} and Ser^{88} abolished its phosphorylation (Figure 2E); and ENO1 was found to be phosphorylated at Ser^{115} and Ser^{282}

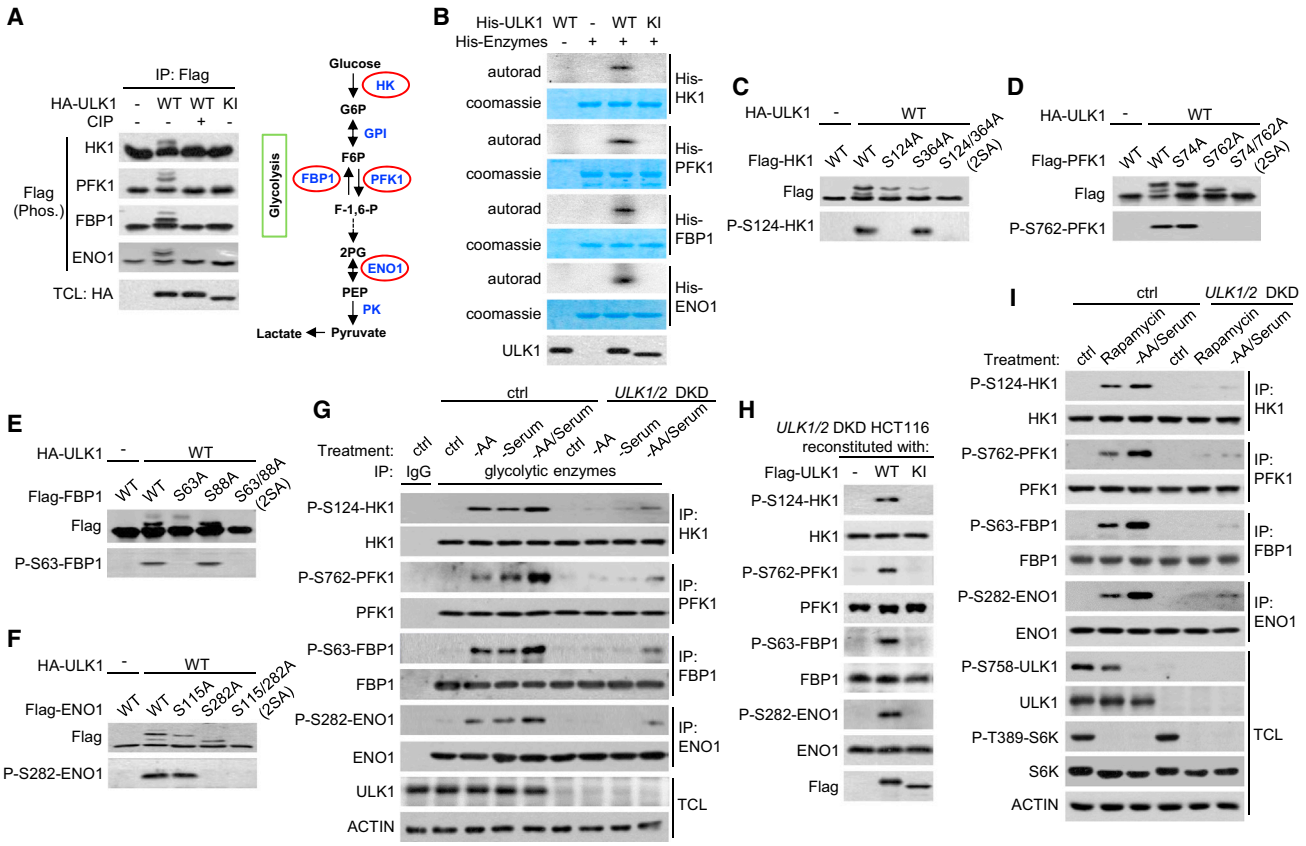

Figure 2. Direct Phosphorylation of Glycolytic Enzymes by ULK1 In Vivo and In Vitro

(A) Changes of the electrophoretic mobility of Flag-tagged HK1, PFK1 (M isoform), FBP1, and ENO1 co-expressed with HA-tagged WT-ULK1 or KI-ULK1 in HEK293T cells on Phos-tag-containing gels (Phos.). CIP, calf-intestinal alkaline phosphatase; TCL, total cell lysates. (Right) Schematic diagram shows the enzymes of glucose metabolic fluxes phosphorylated by ULK1 (circled in red).

(B) In vitro phosphorylation of HK1, PFK1, FBP1, and ENO1 by ULK1.

(C–F) Electrophoretic mobilities of Flag-tagged WT or SA mutants of HK1 (C), PFK1 (D), FBP1 (E), and ENO1 (F) co-expressed with HA-ULK1 in HEK293T cells.

(G) Phosphorylation of metabolic enzymes in control or *ULK1/2* DKD HCT116 cells placed in complete medium or medium free of amino acid and/or serum for 2 hr.

(H) Phosphorylation of metabolic enzymes in *ULK1/2* DKD HCT116 cells reconstituted with Flag-tagged WT-ULK1, KI-ULK1, or empty vector placed in medium free of amino acid and serum for 2 hr.

(I) Phosphorylation of metabolic enzymes in HCT116 cells in complete medium with or without 50 nM rapamycin or in medium free of amino acid and serum for 2 hr.

See also Figure S2.

(Figure 2F). Sequence alignment indicates that most of these serine residues targeted by ULK1 are highly conserved across different species (Figures S2A–S2D). Importantly, the amino acid sequences flanking the phosphorylated residues generally conform to the consensus phosphorylation motif identified previously for the substrates of ULK1 (Egan et al., 2015) or ATG1 (yeast ortholog of ULK1/2; Papinski et al., 2014). Polyclonal antibodies that specifically recognize Ser^{762}-phosphorylated PFK1, Ser^{63}-phosphorylated FBP1, or Ser^{282}-phosphorylated ENO1 was then produced (Figures 2D–2F). Ser^{124}-phosphorylated HK1 happens to be recognized by a commercially available antibody that targets a sequence context-dependent phosphoserine motif (referred here as P-S124-HK1 antibody; Figure 2C). We found that the amount of either the exogenous or endogenous phosphorylated enzymes increases in medium deprived of amino acid and/or serum, whereas knockdown of *ULK1/2* abolished their phosphorylation (Figures 2G and S2E). Furthermore, reconstitution of *ULK1/2* DKD cells with WT-ULK1, but not KI-ULK1, restored the phosphorylation of these enzymes (Figure 2H). Finally, treatment of rapamycin, which is known to active ULK1/2 as a result of inhibition of mTOR, in HCT116 cells also induced the phosphorylation of these enzymes (Figure 2I). These in vitro and in vivo results indicate that ULK1 is a bona fide kinase for HK, PFK1, FBP1, and ENO1.

We next tested whether phosphorylation of these enzymes by ULK1 directly accounts for the changes of their enzymatic activities. Co-expression of ULK1 strongly increased the activity of WT-HK1, whereas the activities of WT forms of PFK1, FBP1, and ENO1 were heavily suppressed by ULK1 (Figures 3A–3E). Meanwhile, the activities of ULK1-nonphosphorylatable mutants

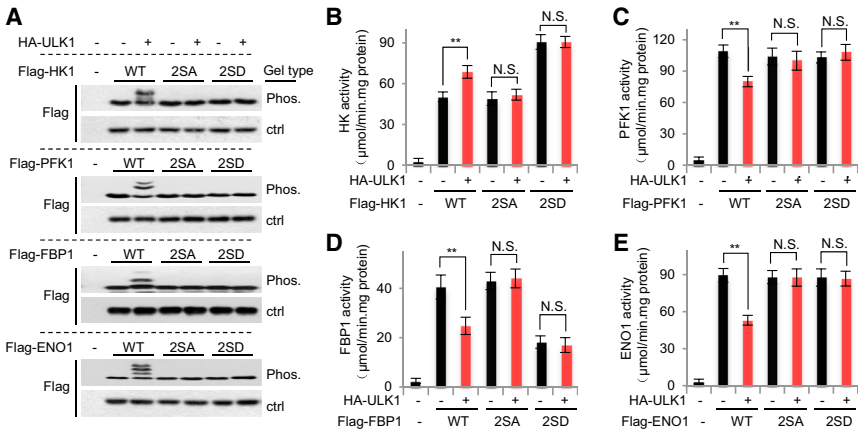

Figure 3. Phosphorylation Modulates the Enzymatic Activities of HK, PFK1, FBP1, and ENO1

(A) Immunoblotting of Flag-tagged enzymes and their mutants co-expressed with HA-tagged ULK1 in HEK293T cells using regular SDS-PAGE gels (ctrl) or Phos-tag-containing gels (Phos.).

(B–E) Enzymatic activities of WT, SA, or SD form of HK (B), PFK1 (M isoform; C), FBP1 (D), and ENO1 (E) assayed with abundant supply of their respective substrates (n = 5 assays).

Error bars denote SEM. Statistical analysis was performed by ANOVA followed by Tukey (**p < 0.01). See also Figure S3.

(SA mutants or 2SA-) of these enzymes were not affected. The serine to aspartate mutants for each enzyme were also created (SD mutants or 2SD-), and it was found that 2SD-HK1 and 2SD-FBP1 can well mimic the phosphorylated states of these two enzymes whereas 2SD-PFK1 and 2SD-ENO1 own prosperities more like their respective SA mutants (Figures 3A–3E). We also determined the Michaelis constant (K_m) values of the enzymes and found that ULK1-mediated phosphorylation had little effect on the binding affinity of each enzyme to its substrate (Figure S3A). The spatial locations of the serine residues targeted by ULK1 are shown in Figure S3B by structural remodeling.

Phosphorylation of HK and FBP1 by ULK1 Sustains Glycolytic Rate whereas ULK1-Mediated Phosphorylation of PFK1 and ENO1 Promotes PPP Flux

To explore the functional consequences of ULK1-mediated phosphorylation of these enzymes of glucose metabolism during nutritional stresses, we first generated HCT116 cell lines in which the expression of HK (including HK1 and HK2), PFK1 (including M, L, and P isoforms), FBP1, or ENO1 was stably knocked down (Figure S4A). As expected, depletion of HK, PFK1, or ENO1 exhibited decreased glucose consumption and lactate production, whereas cells expressing short hairpin RNA (shRNA)-targeting *FBP1* that functions in the gluconeogenic route showed increased glycolytic flux (Figures 4A and S4B; Dong et al., 2013; Li et al., 2014). We then reintroduced WT, SA, or SD forms of HK1, PFK1 (M isoform), FBP1, and ENO1, respectively, into those knockdown cells (Figures 4B–4E). It was found that cells reconstituted with SA mutant of HK1 or FBP1 showed lower levels of glucose uptake and utilization compared to those of the *HK*-KD or *FBP1*-KD cells expressing WT form of HK1 or FBP1 during amino acid and serum starvation (Figures 4F, S4C, and S4D). Meanwhile, cells reconstituted with the phosphor-mimetic SD mutant of HK1 or FBP1 demonstrated constitutively higher capacity in the uptake and utilization of glucose (Figures 4F, S4C, and S4D). In contrast, cells expressing SA or SD mutant of PFK1 or ENO1 exhibited increased glycolytic flux than that of cells expressing their corresponding WT forms in response to starvation (Figures 4G and S4E).

Importantly, the increased HK enzymatic activity and decreased activities of PFK1 and ENO1 during ULK1/2 activation may increase the ratio of glucose flux going through PPP to keep generating reducing forces to eliminate the elevated ROS during amino acid and serum deprivation (Scherz-Shouval et al., 2007). Using [1,2-^{13}C]glucose as a tracer, glycolytic intermediates including G6P/F6P, FBP, GAP/DHAP, 2PG/3PG, PEP, pyruvate and lactate, and PPP intermediates including R5P/X5P, E4P, and S7P were measured by liquid chromatography-tandem mass spectrometry (LC-MS/MS) (Figure S4F). We found that *HK*-KD or *FBP1*-KD cells reconstituted with SA form of HK1 or FBP1 contained lower levels of labeled glycolytic and PPP intermediates than cells reconstituted with their corresponding WT forms cultured in starvation medium, but not in complete medium (Figures 4H, 4I, S4G, and S4H). On the other hand, cells reconstituted with 2SA-PFK1 or 2SA-ENO1 contained lower levels of their corresponding upstream glycolytic intermediates (G6P/F6P for PFK1 and G6P/F6P, FBP, and GAP/DHAP for ENO1) and all the PPP intermediates but higher levels of their corresponding downstream intermediates (FBP, GAP/DHAP, 2PG/3PG, PEP, pyruvate, and lactate for PFK1 and 2PG/3PG, PEP, pyruvate, and lactate for ENO1) than cells reconstituted with their WT counterparts during starvation (Figures 4J, 4K, S4I, and S4J). Meanwhile, we found that 30.6% ± 4.5% of HK1, 38.8% ± 5.2% of PFK1, 25.5% ± 4.0% of FBP1, and 32.1% ± 6.7% of ENO1 are phosphorylated by ULK1/2 after amino acid and growth factor starvation (Figure 4L). Furthermore, *ULK1/2* DKD cells displayed severely decreased intracellular G6P, PEP, pyruvate, and lactate levels during the starvation compared to those in control cells (Figures S4M and S4N).

With the isotope labeling as designed, lactate containing one ^{13}C atom (*) (M+1) is derived only from PPP flux (Figure S4F) whereas lactate containing two ^{13}C atoms (**) (M+2) is mostly derived from direct glycolytic flux without going through PPP. We found that, during amino acid and serum starvation, *PFK1*-KD cells reconstituted with WT-PFK1 displayed higher PPP flux (based on the ratio of lactate* versus lactate**) comparing to *PFK1*-KD cells expressing 2SA-PFK1 (Figure 4M). Similar results were obtained in *ENO1*-KD cells reconstituted with WT-ENO1 and 2SA-ENO1. The differences of PPP flux were not found in those cells cultured in complete medium (Figure S4K). In addition, *HK*-KD or *FBP1*-KD cells expressing SA mutant of HK1 or FBP1 showed similar PPP flux to those cells expressing

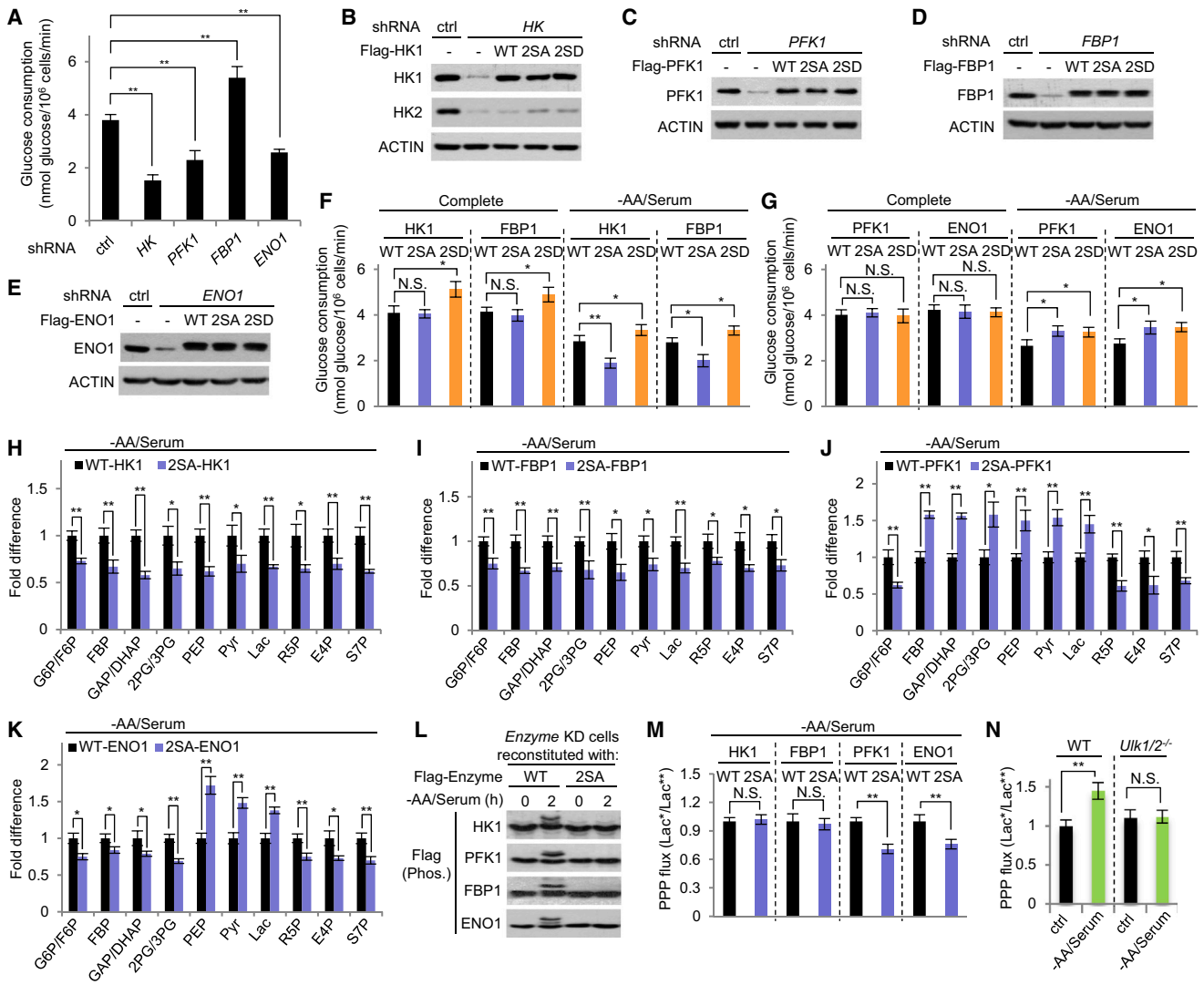

Figure 4. Phosphorylation of Glucose Metabolic Enzymes by ULK1 Sustains Glycolytic Rate and PPP Flux

(A) Glucose consumption of HCT116 cells expressing control shRNA (ctrl) or shRNAs targeting *HK*, *PFK1* (M, L, and P isoform), *FBP1*, or *ENO1* (n = 3 assays).

(B–E) HCT116 cells expressing control shRNA or shRNAs targeting *HK* (B), *PFK1* (M, L, and P isoform; C), *FBP1* (D), or *ENO1* (E) reconstituted with empty vector or WT, SA, or SD form of HK1, PFK1 (M isoform), FBP1, or ENO1.

(F and G) Glucose consumption of cells with knockdown of glucose metabolic enzymes reconstituted with their respective WT, SA, or SD mutant placed in complete medium or medium free of amino acid and serum (n = 4 assays).

(H–K) LC-MS/MS results of labeled intracellular glycolytic and PPP metabolites derived from [1,2-^{13}C]glucose in HCT116 cells with knockdown of *HK* (H), *FBP1* (I), *PFK1* (J), or *ENO1* (K) reconstituted with their respective WT or SA mutant placed in medium free of amino acid and serum (n = 3 experiments). See Supplemental Information for full names of metabolites.

(L) Electrophoretic mobilities of Flag-tagged enzymes in cells as described in (B)–(E) placed in complete medium or medium free of amino acid and serum for 2 hr on Phos-tag-containing gels (Phos.).

(M) LC-MS/MS-based measurement of PPP flux (calculated as the ratio of peak areas of lactate labeled with one ^{13}C carbon [PPP flux] over that labeled with two ^{13}C carbons [direct glycolytic flux without going through PPP] and the first value analyzed is normalized to 1) of HCT116 cells with knockdown of glycolytic enzymes reconstituted with their corresponding WT or SA mutant in medium free of amino acid and serum (n = 3 experiments).

(N) The PPP flux of WT or *Ulk1/2*$^{-/-}$ MEFs placed in complete medium or medium free of amino acid and serum (n = 3 experiments).

Error bars denote SEM. Statistical analysis was performed by ANOVA followed by Tukey in (A), (F), and (G) and by Student's t test in (H)–(N) (*$p < 0.05$; **$p < 0.01$). See also Figure S4.

their corresponding WT forms at all times (Figures 4M and S4K). The PPP results were confirmed by measuring the PPP-dependent $^{14}CO_2$ production from [1-^{14}C]glucose (Figure S4L) and by NMR spectroscopy-based method (Figures S4O and S4P). Importantly, we detected a robust increase in the ratio of PPP flux versus direct glycolytic flux during amino acid and serum

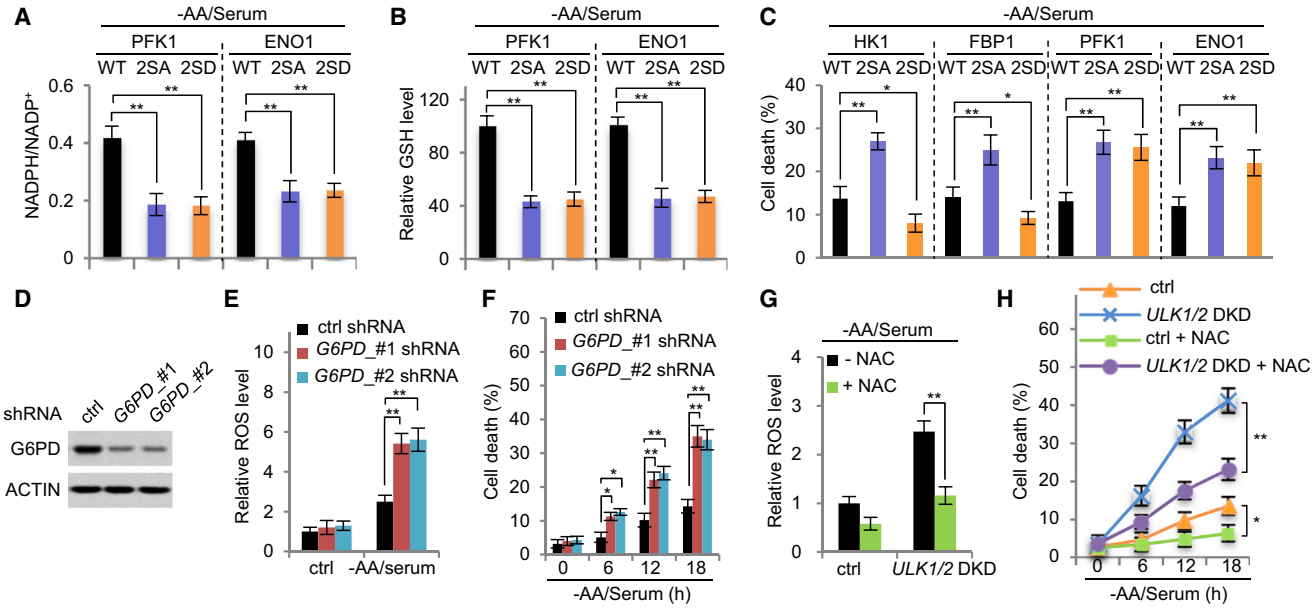

Figure 5. ULK1-Mediated Phosphorylation of Glycolytic Enzymes Protects Cells from ROS-Associated Cell Death

(A–C) Levels of NADPH/NADP$^+$ (A), GSH (B), and cell death rate (C) of cells with knockdown of different enzymes and reconstituted with their corresponding WT, SA, or SD mutant placed in medium free of amino acid and serum (2 hr for A and B; 18 hr for C; n = 3 experiments).

(D) Lentivirus-mediated knockdown of *G6PD* in HCT116 cells.

(E) ROS level of cells expressing control shRNA or shRNA-targeting *G6PD* placed in medium free of amino acid and serum for 2 hr (n = 3 experiments).

(F) Cell death rate of HCT116 cells as described in (D) placed in medium free of amino acid and serum for the indicated periods of time (n = 3 experiments).

(G and H) ROS level and cell death rate of control cells or *ULK1/2* DKD cells placed in medium free of amino acid and serum with or without 2 mM N-acetylcysteine (NAC) (n = 3 experiments).

Error bars denote SEM. Statistical analysis was performed by ANOVA followed by Tukey (*p < 0.05; **p < 0.01). See also Figure S5.

starvation in WT, but not in *Ulk1/2*$^{-/-}$, MEFs (Figures 4N and S4Q). Similarly, knocking down of *ULK1/2* also decreased the PPP flux in U2OS and MCF7 cells during starvation (Figure S4R).

ULK1-Mediated Phosphorylation of Glucose Metabolic Enzymes Protect Cells from ROS-Associated Cell Death

Consistent with the crucial function of PPP in generation of reducing power, intracellular NADPH/NADP$^+$ and GSH levels decreased in *PFK1*-KD or *ENO1*-KD cells expressing SA or SD mutant of PFK1 or ENO1 during starvation comparing to their corresponding WT controls (Figures 5A and 5B). Moreover, much-higher ROS levels and higher percentages of cell death were detected in starved cells with knockdown of enzymes reconstituted with SA mutants of HK1, FBP1, PFK1, or ENO1 than cells expressing their WT counterparts (Figures S5A and 5C). In addition, cells expressing SD mutant of HK1 or FBP1 demonstrate lower ROS and the percentage of cell death than cells expressing the WT form whereas 2SD-PFK1 or 2SD-ENO1 owns prosperities more like their respective SA mutants (Figures S5A and 5C).

Next, we blocked the entry of G6P to PPP by knocking down *G6PD*, the rate-limiting enzyme for PPP (Figure 5D), and found that depletion of G6PD strongly increased the ROS level and accelerated cell death in starved HCT116 cells (Figures 5E and 5F). Finally, addition of antioxidant N-acetylcysteine (NAC) or catalase (CAT) that catalyzes the conversion of hydrogen peroxide to water and oxygen effectively decreased the ROS level and alleviated cell death in *ULK1/2* DKD or *Ulk1/2*$^{-/-}$ cells in response to starvation (Figures 5G, 5H, and S5B).

The higher level of 3PG in cells expressing WT-ENO1 comparing to those expressing 2SA-ENO1 during starvation (Figure 4K) could possibly lead to more-active de novo serine synthesis to further support the production of NADPH (Figure S5C). However, in the absence of amino acids, serine pathway, which requires input from glutamine for transamination reaction, is most likely blocked. Indeed, we found that depletion of PHGDH, the first enzyme directing 3PG to the serine pathway, did not affect ROS, NADPH/NADP$^+$, or cell death level in HCT116 cells during amino acid and serum starvation (Figures S5D–S5H), indicating that serine pathway did not significantly contribute to the production of NADPH under such circumstance.

ULK1/2 Reprogram Glucose Metabolism Independently of Autophagy

To further ascertain an autophagy-independent role of ULK1/2 in the regulation of glucose metabolism, we analyzed the glucose metabolic fluxes in *Atg5*$^{-/-}$ MEFs with or without knockdown of *Ulk1/2*. As previously reported (Kuma et al., 2004), autophagy was deficient in *Atg5*$^{-/-}$ MEFs as monitored with the degradation of p62 and lipidation of microtubule-associated protein 1 light chain 3 (LC3) during amino acid and serum starvation (Figure 6A). We found that, in cells expressing shRNAs targeting *Ulk1/2* in the *Atg5*$^{-/-}$ background, significantly lower glucose consumption, lactate production, and PPP flux could still be

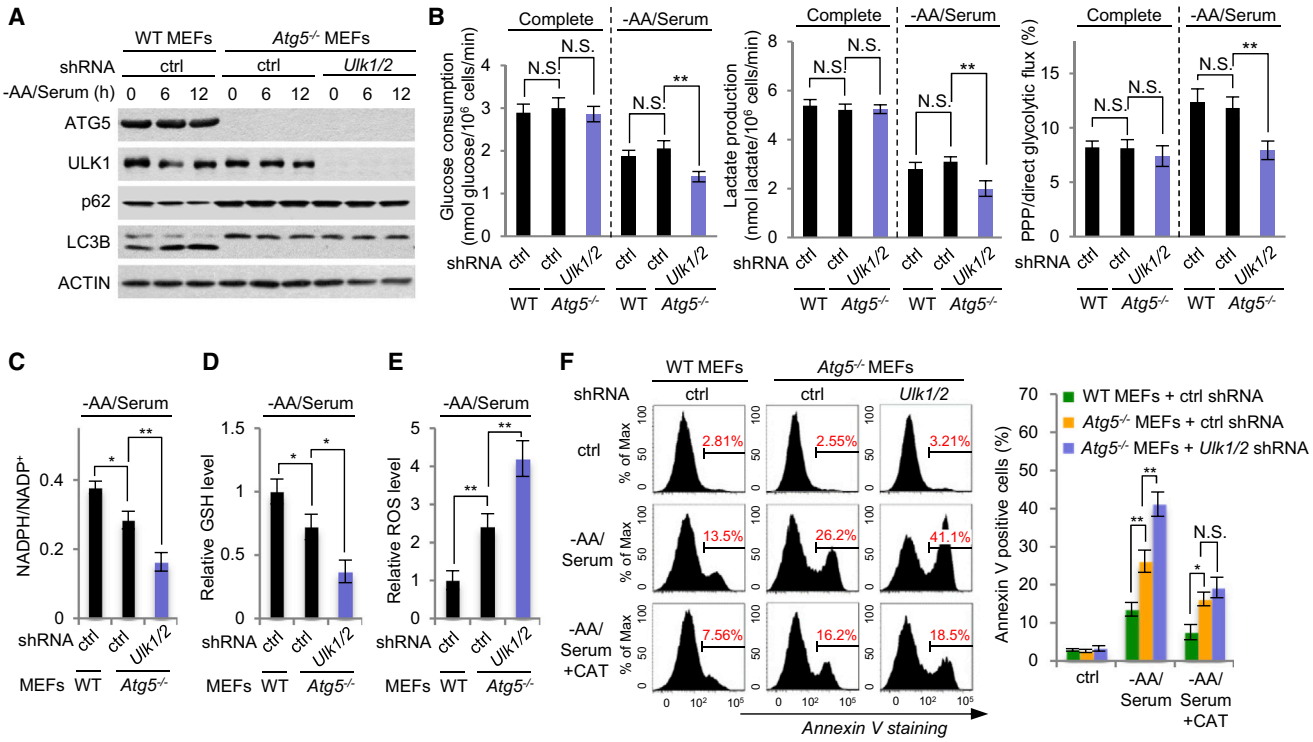

Figure 6. ULK1/2 Reprogram Glucose Metabolism Independently of Autophagy

(A) Lentivirus-mediated knockdown of *Ulk1/2* in *Atg5*$^{-/-}$ MEFs. Cells were placed in medium free of amino acid and serum for the indicated periods of time.

(B) Glucose consumption (left), lactate production (center), and ratio of PPP flux versus the direct glycolytic flux (right) of WT or *Atg5*$^{-/-}$ MEFs expressing control shRNA (ctrl) or shRNAs targeting *Ulk1/2* cultured in complete medium or medium free of amino acid and serum (n = 4 experiments).

(C–E) Levels of NADPH/NADP^{+} (C), GSH (D), and ROS (E) in WT or *Atg5*$^{-/-}$ MEFs expressing control shRNA (ctrl) or shRNAs targeting *Ulk1/2* placed in medium free of amino acid and serum for 2 hr (n = 3 experiments).

(F) Cell death rate of WT or *Atg5*$^{-/-}$ MEFs expressing control shRNA or shRNAs targeting *Ulk1/2* placed in complete medium or medium free of amino acid and serum with or without CAT (600 U/ml) for 18 hr. Statistical results of three independent experiments are shown on the right.

Error bars denote SEM. Statistical analysis was performed by ANOVA followed by Tukey (*p < 0.05; **p < 0.01).

observed under starvation condition (Figure 6B). Moreover, knockdown of *Ulk1/2* in *Atg5*$^{-/-}$ MEFs led to a further decrease of NADPH/NADP^{+} as well as GSH and a further increase of ROS level and percentage of cell death compared to those in *Atg5*$^{-/-}$ MEFs (Figures 6C–6F), and addition of CAT, the antioxidant, strongly alleviated cell death in response to starvation (Figure 6F). These results suggest that, during nutritional stresses, autophagy contributes to the maintenance of cellular redox homeostasis whereas ULK1/2 function simultaneously to further accelerate ROS clearance and enhance cell survival by direct reprogramming of glucose metabolism.

ULK1/2 Maintain Glycolytic Flux, PPP, and Redox Homeostasis at Both Cellular and Organismal Levels

Lacking mitochondria, red blood cells (RBCs) extensively rely on glycolysis for energy production and PPP to generate reducing forces to eliminate ROS from both endogenous and exogenous sources (Beutler, 2008). The ROS would otherwise damage RBCs and impair their ability in oxygen delivery, which contributes to the pathology of a number of diseases (Mohanty et al., 2014; Patra and Hay, 2014). We found that, like *FIP200*$^{-/-}$ mouse embryos (Gan et al., 2006), most of *Ulk1/2*$^{-/-}$ embryos are especially pale at embryonic day 15.5 (E15.5) compared to their WT littermates (Figure S6A). Interestingly, deficiency of *Ulk1* alone, but not *Ulk2*, led to increased accumulation of p62 and the mitochondrial marker protein CoxIV (Figure 7A), confirming an important autophagic role of Ulk1 in erythrocyte maturation (Kundu et al., 2008). However, much-reduced glycolytic flux and PPP activity as well as increased ROS level were detected in RBCs from *Ulk1/2*$^{-/-}$, but not from *Ulk1*$^{-/-}$ or *Ulk2*$^{-/-}$ embryos (Figures 7B, 7C, S6B, and S6C), indicating a complementary but pivotal function of Ulk1 and Ulk2 in the regulation of glucose metabolism of RBCs during embryonic period in vivo. In line with these findings, we found that *Ulk1/2*$^{-/-}$ RBCs are more prone to lysis (Figure S6D) and displayed fractured membrane (Figure S6E). More intriguingly, unlike MEFs and other cells, *Ulk1/2*$^{-/-}$ RBCs display altered glucose utilization even in complete medium (Figure 7B). The critical role of Ulk1 during maturing of RBCs suggests its activation in spite of abundant supply of nutrients around (Kundu et al., 2008). Indeed, we found that, even under complete medium condition, mTORC1 activity in RBCs is maintained in an inactive state (Figure 7D), likely because RBCs lack lysosome, which is essential for mTORC1 activation (Laplante and Sabatini, 2012), allowing Ulk1/2 to be

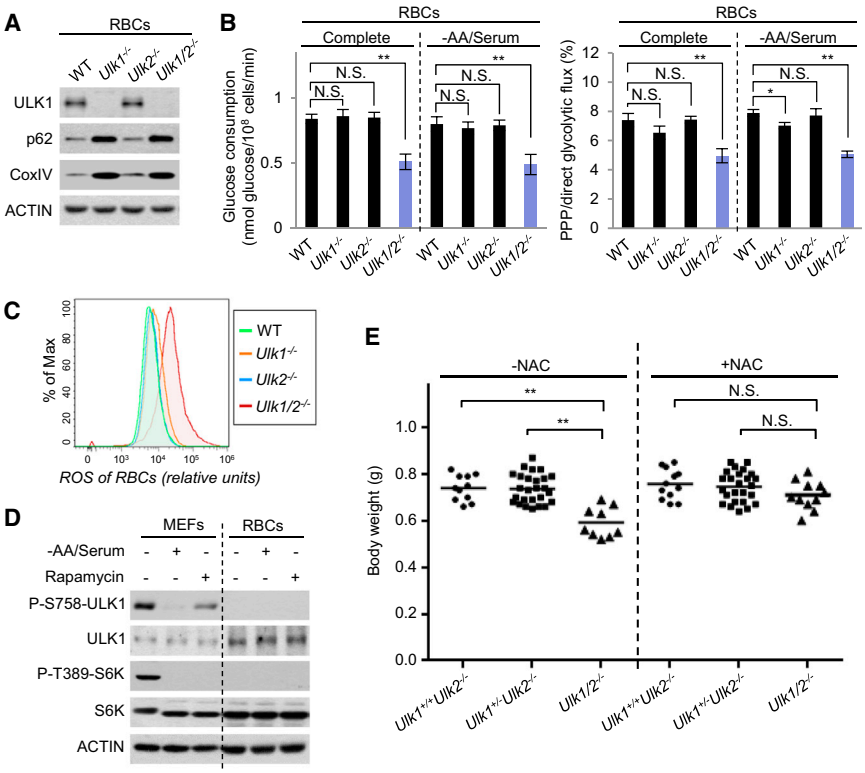

Figure 7. ULK1/2 Maintain Glycolytic Flux, PPP, and Redox Homeostasis at Both Cellular and Organismal Levels

(A) Red blood cells (RBCs) from embryos of different genotypes were extracted and subjected to immunoblotting.

(B) Glucose consumption (left) and ratio of PPP flux versus the direct glycolytic flux (right) of RBCs from embryos of different genotypes placed in complete medium or medium free of amino acid and serum (n = 4 experiments).

(C) Representative ROS level of RBCs from embryos of different genotypes.

(D) Cell lysates of WT MEFs or WT RBCs placed in complete medium or medium free of amino acid and serum for 2 hr or treated with 50 nM rapamycin for 2 hr in complete medium were immunoblotted as indicated.

(E) Weights of the embryos of *Ulk1*$^{+/+}$*Ulk2*$^{-/-}$, *Ulk1*$^{+/-}$*Ulk2*$^{-/-}$, and *Ulk1/2*$^{-/-}$ at embryonic day 15.5 (E15.5) from *Ulk1*$^{+/-}$*Ulk2*$^{-/-}$ mouse parents. During the breeding, half of the mice had access to normal water and the other half to water supplemented with 40 mM NAC. Only litters containing *Ulk1/2*$^{-/-}$ embryos were included in the analysis.

(F) Model for ULK1/2-mediated regulation of glucose metabolic fluxes.

Error bars denote SEM. Statistical analysis was performed by ANOVA followed by Tukey in (B) and (E) (*$p < 0.05$; **$p < 0.01$). See also Figure S6.

DISCUSSION

In this study, we demonstrate a model that, under deprivation of amino acid and growth factors, the autophagy-initiation kinases ULK1/2 act as a key signaling node to sustain glycolysis and at the same time repartition more carbon flux to PPP through phosphorylating multiple enzymes in the glucose metabolic pathways, including HK, PFK1, FBP1, and ENO1 (Figure 7F). On one hand, phosphorylation of HK renders its enzymatic activity increased, promoting the conversion of glucose to G6P and subsequently glucose uptake, such that the glycolytic flux is sustained in control cells compared to cells depleted of ULK1/2 under the same nutritional stresses. It is also important to note that, because HK is product inhibited by G6P, the increase in the V_{max} of HK by ULK1/2-mediated phosphorylation could probably compensate for the higher product inhibition of G6P in ULK1/2-containing cells during starvation. Meanwhile, the reduced activity of FBP1 after ULK1/2-dependent phosphorylation minimizes the reversal of F-1,6-P back to F6P, indirectly drawing more glucose toward catabolism.

On the other hand, ULK1/2-mediated phosphorylation of PFK1 and ENO1 inhibits their enzymatic activity and modulates glycolytic flux in an opposite way comparing to the effects of HK and FBP1 when assayed individually (Figures 4F, 4G, S4C,

constantly activated. Next, we used NAC, the ROS scavenger, to test whether administration of this antioxidant could rescue the defects of *Ulk1/2*$^{-/-}$ embryos. In consonance with the results obtained in HCT116 and MEFs showing that addition of NAC or the other antioxidant, CAT, effectively decreased the ROS level and mitigated cell death in *ULK1/2* DKD or *Ulk1/2*$^{-/-}$ cells during nutrient starvation (Figures 5G, 5H, and S5B), we found that supply of NAC alleviated the paleness of *Ulk1/2*$^{-/-}$ embryos (Figure S6F). Moreover, we found that the body weight of *Ulk1/2*$^{-/-}$ mouse embryos (Cheong et al., 2014) was also restored to normal range in response to the supply of NAC (Figure 7E). These results demonstrate that the failure in the maintenance of a regular PPP flux, which further leads to the disrupted redox balance, is the major cause for the many defects of *Ulk1/2*$^{-/-}$ embryos.

and S4E). A critical issue would be how the inhibition of PFK1 and ENO1 activity by ULK1/2 can be reconciled to the sustained glycolysis observed in WT cells (Figures 1A, 1B, and S1C–S1E). One possibility is that the contribution of phosphorylated HK1 and FBP1 in stimulating overall glycolysis may override the opposite effects caused by inhibition of PFK1 and ENO1 as the varied enzymatic activities after phosphorylation by ULK1/2 sum up to sustain glycolysis under nutritional stress. It is also formally possible that ULK1/2 can phosphorylate more as-yet-unidentified substrates involved in glucose metabolism, which would await advent of a complete plethora of the targets of ULK1/2. Nevertheless, it is clear that inhibition of the enzymatic activities of PFK1 and ENO1 acts to maintain the level of G6P based on our metabolomic studies and thereby likely to divert relatively more glucose flux to PPP (Figures 4J–4M, S4L, and S4P). Previous work showed that inhibition of PFK1 by O-GlcNAcylation during hypoxia promotes PPP activity and enhances cell survival (Yi et al., 2012), emphasizing the importance of repression of PFK1 in maintaining PPP activity during stresses. Another concern is that the blunted ENO1 activity after ULK1/2-mediated phosphorylation may have an adverse effect on the processing of intermediates recovered from the non-oxidative branch of PPP. In fact, the intermediates from PPP in the form of GAP and F6P can also be converted back to G6P and replenish the oxidative branch of PPP (Riganti et al., 2012), forming a closed cycle of PPP that excludes ENO1 activity under circumstances such as nutrient deprivation when large amount of NADPH is needed, such that a relatively higher PPP flux can be continuously maintained (Figures 4M, S4L, and S4P). In support of the above notion is that suppression of pyruvate kinase M2, which is located downstream of ENO1 in the glycolytic pathway, diverts more glucose to PPP in response to oxidative stress (Anastasiou et al., 2011).

It is commonly believed that gluconeogenesis occurs mostly in hepatic and renal cells (Scrutton and Utter, 1968). Indeed, we found that FBP1 activity in MEFs is too low to be detected. However, the expression of certain gluconeogenic enzymes including PEP carboxykinase and FBP1 has been reported in a variety of other type of cells originated from tissues including prostate, stomach, lung, and small intestine (Yánez et al., 2003). For example, human breast cancer MCF7 cells express functional and significant amount of FBP1 (Dong et al., 2013). Moreover, we detected both basal protein level and S63-phosphorylated FBP1 in HCT116 cells and cells expressing shRNA-targeting endogenous FBP1 showed increased glucose consumption and lactate production by approximately 37% (Figures 4A and S4B), which is consistent with the finding that genetic loss of FBP1 often causes sudden infant death characterized by hypoglycemia and lactic acidosis (Emery et al., 1988). These results confirm the existence of meaningful FBP1 in some cancer lines to impact glucose metabolism. Meanwhile, the phosphorylation of FBP1 may not only affect the rate of the reaction of F-1,6-P back to F6P in glycolysis but also impinge on other functions of FBP1 such as its modulation of the nuclear hypoxia-inducible factor (HIF) (Li et al., 2014), although it was shown that expression levels of FBP1 play a dominant role in this process. Of note, the activation or inhibition of FBP1 can only affect the absolute values of PPP flux, which is indirectly caused by the altered glucose consumption rate but cannot affect the ratio of PPP flux versus glycolytic flux.

Autophagy plays a critical role for cell survival in response to nutrient deprivation and various other stresses (Galluzzi et al., 2014; Rabinowitz and White, 2010; Xie and Klionsky, 2007). Meanwhile, under many conditions such as amino acid and growth factor deprivation, the utilization of glucose in the environment could also be tightly regulated and vital for cell fate determination. Importantly, as glucose is transported by facilitated diffusion, which is a passive transport process, and our "starvation medium" contains a regular concentration of glucose, it is thus rational for the cells to intake glucose even in the absence of amino acid and serum. Indeed, we found that, although the rate of glucose consumption decreased in response to amino acid and serum starvation in WT cells, depletion of ULK1/2 led to a further significantly lower glucose consumption rate (Figures 1A, 1B, and S1C–S1E). Consistently, knockout of *FIP200*, an essential gene for the kinase activity of endogenous ULK1/2 (Hara et al., 2008), reduces glucose uptake and intracellular lactate production in mammary tumor cells (Wei et al., 2011), pointing to a crucial role of ULK1/2 complexes in sustaining glycolytic flux. Moreover, we found that the function of ULK1/2 in the regulation of glucose metabolism does not rely on downstream autophagic events (Figure 6). In addition, ATG7, another critical factor of the autophagy core machinery, has been reported to regulate p53-dependent cell cycle and cell death pathways independently of autophagy during metabolic stress (Lee et al., 2012). These evidences suggest that multi-functionality could be a common feature for autophagic-related genes.

Altogether, we have identified an adaptive mechanism for the reprogramming of glucose metabolism in response to amino acid and growth factor deprivation, in which ULK1/2 function by simultaneously altering the enzymatic activities of multiple glycolytic enzymes to sustain the production of energy and reducing forces and thus maintain the overall metabolic homeostasis besides their classical role in autophagy. An increasing body of evidence demonstrates that disrupted cellular glucose metabolic and redox balance tightly links with various pathological disorders (DeBerardinis and Thompson, 2012; Kawagishi and Finkel, 2014; Levine and Puzio-Kuter, 2010; Vander Heiden et al., 2009). Elucidation of the functions of ULK1/2 in glucose catabolism may therefore provide new therapeutic strategies for prevention and treatment of human metabolic diseases.

EXPERIMENTAL PROCEDURES

For detailed protocols, see Supplemental Experimental Procedures.

Cell Culture, Transient Transfection, Lentivirus Infection, Immunoprecipitation, Western Blotting, and Animal Care

HCT116, HEK293T, and MEFs were maintained in DMEM supplemented with 10% fetal bovine serum (FBS), 2 mM L-glutamine, 100 IU penicillin, and 100 mg/ml streptomycin at 37°C in a humidified incubator containing 5% CO_2. For amino acid and serum starvation medium, unless otherwise specified, Earle's Balanced Salts Solution (EBSS) (cat. 24010-043; GIBCO) was supplemented with 0.25% BSA, glucose, vitamins, and minerals at the same concentrations as in DMEM. Polyethylenimine at a final concentration of 10 μM was used to transfect HEK293T cells. Transfected cells were harvested at 24 hr after transfection. Lentiviruses for infection of HCT116 and MEFs were

packaged in HEK293T cells using Lipofectamine 2000 transfection. Thirty hours after transfection, medium was collected and added to the target cells. Cell lysis, immunoprecipitation (IP), and western blotting were carried out as previously described (Lin et al., 2012). All animal experiments were approved by the Institutional Animal Care and Use Committee at Xiamen University.

Statistical Analysis

For experiments with only two groups, Student's t test was used for statistical comparisons. ANOVA with Tukey's post-test (one-way ANOVA for comparisons between groups; two-way ANOVA for comparisons of magnitude of changes between different groups from different cell lines or treatments) was used to compare values among different experimental groups using the SPSS Statistics 17.0 program. $p < 0.05$ was considered as statistically significant (*) and $p < 0.01$ as highly significant (**).

SUPPLEMENTAL INFORMATION

Supplemental Information includes Supplemental Experimental Procedures and six figures and can be found with this article at http://dx.doi.org/10.1016/j.molcel.2016.04.009.

AUTHOR CONTRIBUTIONS

T.Y.L., Y.Sun, Y.Liang, and S.-C.L. conceived the project and designed the experiments. T.Y.L., Y. Sun., Y.Liang, Q.L., Y. Shi, C.-S.Z., C.Z., L.S., P.Z., X.Z., Y.-Q.W., S.C., M.J., C.C., and C.X. performed experiments and participated in discussion of the results. X.L. and T.C. helped with generation of antibodies. H.-Y.H. helped with NMR analyses. X.H., Y.W., Y.Lin, and S.Z. contributed to metabolites measurements. T.Y.L., Y.Sun, J.Y.Y., Z.Y., S.-Y.L., D.T.C., and S.-C.L. analyzed data and wrote the paper.

ACKNOWLEDGMENTS

We thank Dr. N. Mizushima for providing *Atg5*$^{-/-}$ MEFs and Dr. D. Zhou, Dr. Y. Li, and Dr. H.R. Wang for useful discussions. This work was supported by the State Key Program of National Natural Science of China (no. 31130016), the 973 Program (no. 2011CB910800, no. 2013CB530600, and no. 2014CB910602), National Natural Science Foundation of China for Fostering Talents in Basic Research (no. J1310027), the Foundation for Innovative Research Groups of the National Natural Science Foundation of China (no. 31221065), and the 111 Project of Education of China (no. B06016).

Received: October 12, 2015
Revised: March 9, 2016
Accepted: April 5, 2016
Published: May 5, 2016

REFERENCES

Anastasiou, D., Poulogiannis, G., Asara, J.M., Boxer, M.B., Jiang, J.K., Shen, M., Bellinger, G., Sasaki, A.T., Locasale, J.W., Auld, D.S., et al. (2011). Inhibition of pyruvate kinase M2 by reactive oxygen species contributes to cellular antioxidant responses. Science *334*, 1278–1283.

Bensaad, K., Tsuruta, A., Selak, M.A., Vidal, M.N.C., Nakano, K., Bartrons, R., Gottlieb, E., and Vousden, K.H. (2006). TIGAR, a p53-inducible regulator of glycolysis and apoptosis. Cell *126*, 107–120.

Beutler, E. (2008). Glucose-6-phosphate dehydrogenase deficiency: a historical perspective. Blood *111*, 16–24.

Cheong, H., Wu, J., Gonzales, L.K., Guttentag, S.H., Thompson, C.B., and Lindsten, T. (2014). Analysis of a lung defect in autophagy-deficient mouse strains. Autophagy *10*, 45–56.

Choi, A.M., Ryter, S.W., and Levine, B. (2013). Autophagy in human health and disease. N. Engl. J. Med. *368*, 651–662.

DeBerardinis, R.J., and Thompson, C.B. (2012). Cellular metabolism and disease: what do metabolic outliers teach us? Cell *148*, 1132–1144.

Díaz-Ramos, A., Roig-Borrellas, A., García-Melero, A., and López-Alemany, R. (2012). α-Enolase, a multifunctional protein: its role on pathophysiological situations. J. Biomed. Biotechnol. *2012*, 156795.

Dong, C., Yuan, T., Wu, Y., Wang, Y., Fan, T.W., Miriyala, S., Lin, Y., Yao, J., Shi, J., Kang, T., et al. (2013). Loss of FBP1 by Snail-mediated repression provides metabolic advantages in basal-like breast cancer. Cancer Cell *23*, 316–331.

Egan, D.F., Shackelford, D.B., Mihaylova, M.M., Gelino, S., Kohnz, R.A., Mair, W., Vasquez, D.S., Joshi, A., Gwinn, D.M., Taylor, R., et al. (2011). Phosphorylation of ULK1 (hATG1) by AMP-activated protein kinase connects energy sensing to mitophagy. Science *331*, 456–461.

Egan, D.F., Chun, M.G., Vamos, M., Zou, H., Rong, J., Miller, C.J., Lou, H.J., Raveendra-Panickar, D., Yang, C.C., Sheffler, D.J., et al. (2015). Small molecule inhibition of the autophagy kinase ULK1 and identification of ULK1 substrates. Mol. Cell *59*, 285–297.

Emery, J.L., Howat, A.J., Variend, S., and Vawter, G.F. (1988). Investigation of inborn errors of metabolism in unexpected infant deaths. Lancet *2*, 29–31.

Fan, J., Ye, J., Kamphorst, J.J., Shlomi, T., Thompson, C.B., and Rabinowitz, J.D. (2014). Quantitative flux analysis reveals folate-dependent NADPH production. Nature *510*, 298–302.

Galluzzi, L., Pietrocola, F., Levine, B., and Kroemer, G. (2014). Metabolic control of autophagy. Cell *159*, 1263–1276.

Gan, B., Peng, X., Nagy, T., Alcaraz, A., Gu, H., and Guan, J.L. (2006). Role of FIP200 in cardiac and liver development and its regulation of TNFalpha and TSC-mTOR signaling pathways. J. Cell Biol. *175*, 121–133.

Hammerman, P.S., Fox, C.J., and Thompson, C.B. (2004). Beginnings of a signal-transduction pathway for bioenergetic control of cell survival. Trends Biochem. Sci. *29*, 586–592.

Hara, T., Takamura, A., Kishi, C., Iemura, S., Natsume, T., Guan, J.L., and Mizushima, N. (2008). FIP200, a ULK-interacting protein, is required for autophagosome formation in mammalian cells. J. Cell Biol. *181*, 497–510.

Hosokawa, N., Hara, T., Kaizuka, T., Kishi, C., Takamura, A., Miura, Y., Iemura, S., Natsume, T., Takehana, K., Yamada, N., et al. (2009a). Nutrient-dependent mTORC1 association with the ULK1-Atg13-FIP200 complex required for autophagy. Mol. Biol. Cell *20*, 1981–1991.

Hosokawa, N., Sasaki, T., Iemura, S., Natsume, T., Hara, T., and Mizushima, N. (2009b). Atg101, a novel mammalian autophagy protein interacting with Atg13. Autophagy *5*, 973–979.

Jung, C.H., Jun, C.B., Ro, S.H., Kim, Y.M., Otto, N.M., Cao, J., Kundu, M., and Kim, D.H. (2009). ULK-Atg13-FIP200 complexes mediate mTOR signaling to the autophagy machinery. Mol. Biol. Cell *20*, 1992–2003.

Kawagishi, H., and Finkel, T. (2014). Unraveling the truth about antioxidants: ROS and disease: finding the right balance. Nat. Med. *20*, 711–713.

Kim, J., Kundu, M., Viollet, B., and Guan, K.L. (2011). AMPK and mTOR regulate autophagy through direct phosphorylation of Ulk1. Nat. Cell Biol. *13*, 132–141.

Kinoshita, E., Kinoshita-Kikuta, E., Takiyama, K., and Koike, T. (2006). Phosphate-binding tag, a new tool to visualize phosphorylated proteins. Mol. Cell. Proteomics *5*, 749–757.

Kuma, A., Hatano, M., Matsui, M., Yamamoto, A., Nakaya, H., Yoshimori, T., Ohsumi, Y., Tokuhisa, T., and Mizushima, N. (2004). The role of autophagy during the early neonatal starvation period. Nature *432*, 1032–1036.

Kundu, M., Lindsten, T., Yang, C.Y., Wu, J., Zhao, F., Zhang, J., Selak, M.A., Ney, P.A., and Thompson, C.B. (2008). Ulk1 plays a critical role in the autophagic clearance of mitochondria and ribosomes during reticulocyte maturation. Blood *112*, 1493–1502.

Laplante, M., and Sabatini, D.M. (2012). mTOR signaling in growth control and disease. Cell *149*, 274–293.

Lee, I.H., Kawai, Y., Fergusson, M.M., Rovira, I.I., Bishop, A.J.R., Motoyama, N., Cao, L., and Finkel, T. (2012). Atg7 modulates p53 activity to regulate cell cycle and survival during metabolic stress. Science *336*, 225–228.

Levine, A.J., and Puzio-Kuter, A.M. (2010). The control of the metabolic switch in cancers by oncogenes and tumor suppressor genes. Science *330*, 1340–1344.

Li, B., Qiu, B., Lee, D.S., Walton, Z.E., Ochocki, J.D., Mathew, L.K., Mancuso, A., Gade, T.P., Keith, B., Nissim, I., and Simon, M.C. (2014). Fructose-1,6-bisphosphatase opposes renal carcinoma progression. Nature *513*, 251–255.

Lin, S.Y., Li, T.Y., Liu, Q., Zhang, C., Li, X., Chen, Y., Zhang, S.M., Lian, G., Liu, Q., Ruan, K., et al. (2012). GSK3-TIP60-ULK1 signaling pathway links growth factor deprivation to autophagy. Science *336*, 477–481.

Mizushima, N., Yoshimori, T., and Ohsumi, Y. (2011). The role of Atg proteins in autophagosome formation. Annu. Rev. Cell Dev. Biol. *27*, 107–132.

Mohanty, J.G., Nagababu, E., and Rifkind, J.M. (2014). Red blood cell oxidative stress impairs oxygen delivery and induces red blood cell aging. Front. Physiol. *5*, 84.

Mor, I., Cheung, E.C., and Vousden, K.H. (2011). Control of glycolysis through regulation of PFK1: old friends and recent additions. Cold Spring Harb. Symp. Quant. Biol. *76*, 211–216.

Nakatogawa, H., Suzuki, K., Kamada, Y., and Ohsumi, Y. (2009). Dynamics and diversity in autophagy mechanisms: lessons from yeast. Nat. Rev. Mol. Cell Biol. *10*, 458–467.

Papinski, D., Schuschnig, M., Reiter, W., Wilhelm, L., Barnes, C.A., Maiolica, A., Hansmann, I., Pfaffenwimmer, T., Kijanska, M., Stoffel, I., et al. (2014). Early steps in autophagy depend on direct phosphorylation of Atg9 by the Atg1 kinase. Mol. Cell *53*, 471–483.

Patra, K.C., and Hay, N. (2014). The pentose phosphate pathway and cancer. Trends Biochem. Sci. *39*, 347–354.

Rabinowitz, J.D., and White, E. (2010). Autophagy and metabolism. Science *330*, 1344–1348.

Riganti, C., Gazzano, E., Polimeni, M., Aldieri, E., and Ghigo, D. (2012). The pentose phosphate pathway: an antioxidant defense and a crossroad in tumor cell fate. Free Radic. Biol. Med. *53*, 421–436.

Russell, R.C., Tian, Y., Yuan, H., Park, H.W., Chang, Y.Y., Kim, J., Kim, H., Neufeld, T.P., Dillin, A., and Guan, K.L. (2013). ULK1 induces autophagy by phosphorylating Beclin-1 and activating VPS34 lipid kinase. Nat. Cell Biol. *15*, 741–750.

Scherz-Shouval, R., Shvets, E., Fass, E., Shorer, H., Gil, L., and Elazar, Z. (2007). Reactive oxygen species are essential for autophagy and specifically regulate the activity of Atg4. EMBO J. *26*, 1749–1760.

Scrutton, M.C., and Utter, M.F. (1968). The regulation of glycolysis and gluconeogenesis in animal tissues. Annu. Rev. Biochem. *37*, 249–302.

Shang, L., Chen, S., Du, F., Li, S., Zhao, L., and Wang, X. (2011). Nutrient starvation elicits an acute autophagic response mediated by Ulk1 dephosphorylation and its subsequent dissociation from AMPK. Proc. Natl. Acad. Sci. USA *108*, 4788–4793.

Vander Heiden, M.G., Cantley, L.C., and Thompson, C.B. (2009). Understanding the Warburg effect: the metabolic requirements of cell proliferation. Science *324*, 1029–1033.

Wang, Z.V., Rothermel, B.A., and Hill, J.A. (2010). Autophagy in hypertensive heart disease. J. Biol. Chem. *285*, 8509–8514.

Wei, H., Wei, S., Gan, B., Peng, X., Zou, W., and Guan, J.L. (2011). Suppression of autophagy by FIP200 deletion inhibits mammary tumorigenesis. Genes Dev. *25*, 1510–1527.

Wellen, K.E., and Thompson, C.B. (2012). A two-way street: reciprocal regulation of metabolism and signalling. Nat. Rev. Mol. Cell Biol. *13*, 270–276.

Wilson, J.E. (2003). Isozymes of mammalian hexokinase: structure, subcellular localization and metabolic function. J. Exp. Biol. *206*, 2049–2057.

Xie, Z., and Klionsky, D.J. (2007). Autophagosome formation: core machinery and adaptations. Nat. Cell Biol. *9*, 1102–1109.

Yánez, A.J., Nualart, F., Droppelmann, C., Bertinat, R., Brito, M., Concha, I.I., and Slebe, J.C. (2003). Broad expression of fructose-1,6-bisphosphatase and phosphoenolpyruvate carboxykinase provide evidence for gluconeogenesis in human tissues other than liver and kidney. J. Cell. Physiol. *197*, 189–197.

Yi, W., Clark, P.M., Mason, D.E., Keenan, M.C., Hill, C., Goddard, W.A., 3rd, Peters, E.C., Driggers, E.M., and Hsieh-Wilson, L.C. (2012). Phosphofructokinase 1 glycosylation regulates cell growth and metabolism. Science *337*, 975–980.